

Effects of Supercritical CO₂ Fluids on Pore Morphology of Coal: Implications for CO₂ Geological Sequestration

Kaizhong Zhang,^{†,‡,§} Yuanping Cheng,^{*,†,‡,§} Kan Jin,^{†,‡,§} Haijun Guo,^{†,‡,§} Qingquan Liu,^{†,‡,§} Jun Dong,^{†,‡,§} and Wei Li^{†,‡,§}

[†]Key Laboratory of Coal Methane and Fire Control, Ministry of Education, China University of Mining and Technology, Xuzhou, Jiangsu 221116, China

[‡]National Engineering Research Center of Coal Gas Control, China University of Mining and Technology, Xuzhou, Jiangsu 221116, China

[§]School of Safety Engineering, China University of Mining and Technology, Xuzhou 221116, China

ABSTRACT: A systematic knowledge of the pore morphology of coal treated with supercritical CO₂ (ScCO₂) is critical for the process of CO₂ geological sequestration. To better understand the desorption mechanism and to evaluate the storage capacity of target coal seams, the changes in pore volume, pore size distribution, fractal dimension, pore shape, and connectivity in high-, middle-, and low-rank coals were analyzed using N₂/CO₂ adsorption and mercury intrusion porosimetry. The results indicate that micropores of high- and middle-rank coals decreased after ScCO₂ treatment, whereas an increasing trend was found in low-rank coals, and ScCO₂ promoted the accessibility of the macropore spaces for all coals. With ScCO₂ treatment, the roughness of smaller pores in both high- and middle-rank coals decreased, whereas larger pores became more complex for high-rank coals. Although no significant change was observed in the pore shapes, ScCO₂ facilitated the development of effective pore spaces and improved the connectivity of the pore system. Additionally, the gas desorption properties of these samples were enhanced by ScCO₂, verifying the pore morphology results. A conceptual model was proposed to explain the mechanism of the desorption process in relation to the constricted pore spaces of the coal matrix under ScCO₂ and higher-pressure conditions. The results contribute to the understanding of long-term CO₂ storage and enhanced coalbed methane recovery.

1. INTRODUCTION

In recent years, considerable attention has been paid to the greenhouse gases (particularly CO₂) produced by the combustion of carbon-based fuels.¹ To overcome this challenge, carbon capture and storage (CCS) technology has been used to prevent CO₂ emissions into the atmosphere, which is considered to be the only way to significantly and immediately influence the atmospheric CO₂ level.² Among the various storage options, including oil and gas reservoirs, deep saline aquifers, and unmineable coal seams, storage in coal seams is one of the most promising opportunities for long-term sequestration^{3–5} because it offers the following advantages: (1) Unmineable deep coal seams are one of the most common potential disposal sites globally and generally locate near large point sources of CO₂ emission. (2) The injection of CO₂ into coal seams contributes to CO₂ enhanced coalbed methane recovery (ECBM). (3) CO₂ can be absorbed in coal with long-term stability. To better understand the process of CO₂ sequestration in coal and to predict the reliability of long-term storage, it is worthwhile to evaluate the storage capacity of coal seams. A limited number of studies on the CO₂ adsorption–desorption mechanism of ScCO₂ condition have been reported.^{6–9}

The sorption, flow, and transport behaviors of fluids are influenced by the effects of pore morphology, i.e., the pore system of coal seams, which is the key to understanding the adsorption–desorption mechanism during long-term storage.^{10,11} Generally, pore morphology encompasses pore volume, surface area, pore size distribution (PSD), pore

shape, connectivity, and fractal dimension.¹² On the basis of the IUPAC classification,^{13,14} the current studies categorize coal pores as micropores (<2 nm), mesopores (2–50 nm), and macropores (>50 nm). Numerous studies^{15–18} have measured pore morphology under normal (subcritical) conditions via physical adsorption, small-angle X-ray scattering (SAXS), scanning electron microscopy (SEM), mercury intrusion porosimetry (MIP), and nuclear magnetic resonance spectroscopy (NMR). Among these methods, physical adsorption and MIP have been proven to be effective techniques to characterize the smaller and larger pores in coal, respectively.¹⁹ Other studies on coal pore morphology have demonstrated that there is an interconnected pore network with higher surface area and more diverse types of pores (open pores, half-open pores, and closed pores) in coals than that in conventional rocks.^{20,21} Coal contains constricted pore spaces, which occur on all scales (micropores, mesopores, and macropores).²²

For conventional CO₂, it has been demonstrated that CO₂ molecules are absorbed into the coal structure, i.e., uptake, resulting in swelling of the coal matrix.²³ This phenomenon may cause a decrease in the fracture aperture and permeability in the pore system.²⁴ However, when injected into coal seams below 800 m, the temperature and pressure of the coal seams for geological sequestration are above the critical points of CO₂ ($T_c = 31.8$ °C, $P_c = 7.38$ MPa).²⁵ Under these supercritical

Received: December 5, 2016

Revised: March 5, 2017

Published: April 18, 2017

conditions, which are completely different from normal conditions, the interactions of CO₂ with coal and the effects of CO₂ on the properties of coal are very complicated. Coal, as a porous medium, is a cross-linked macromolecular network structure containing moisture, mineral substances, organic matter, and a complex pore network. The coal structure can be regarded as glassy, brittle, and hard.²⁶ However, when exposed to ScCO₂ over a period of time, the coal structure is transformed into a rubbery material with more flexible chains and networks, causing rearrangement of the structure.^{27,28} Another effect is swelling, which reaches a maximum at temperatures between 25 and 55 °C and pressures of approximately 8–10 MPa and does not change beyond these points.²⁹ Thus, this effect is not likely to produce further significant changes in the pore size of coals under ScCO₂. Additionally, accompanied by the existence of water in the coal seam, CO₂ injection may reduce the overall pH.³⁰ ScCO₂ has an ability to extract organic matter from coals, and if mixed with water, it can also dissolve inorganic material, which contributes to changes in the pore structure.^{31,32}

Considering the above effects on the coal structure, it is essential to explain the changes in pore morphology during CO₂ sequestration in coal seams. However, limited research has focused on this topic, especially the comprehensive and systematic analysis of micropores, mesopores, and macropores during CO₂ sequestration. Moreover, a novel conceptual model is required to explain the migration mechanism of CO₂ molecules in the constricted pore spaces of the coal matrix, which may help to understand the effect of coal structure changes on the mechanism of adsorption–desorption during CO₂ sequestration.

In this study, the effects of ScCO₂ on the pore morphology of high-, middle-, and low-rank coals were investigated through CO₂ adsorption, N₂ adsorption, and MIP to comprehensively and systematically analyze the changes in micropores, mesopores, and macropores. The main focus of this study was analysis of the pore volume, PSD, fractal dimension, pore shape, and connectivity before and after ScCO₂ treatment. Additionally, desorption property tests were performed to verify the influence of ScCO₂ on the changes in pore morphology, and the mechanism of desorption process was analyzed to investigate the influences on long-term CO₂ storage.

2. EXPERIMENTAL SECTION

2.1. Sample Preparation. Three metamorphic grade coal samples were sampled from Wolonghu coal mine in the Wanbei coalfield, Haizi coal mine in the Huaibei coalfield, and Dalong coal mine in the Tiefa coalfield in China, representing different coal ranks of anthracite (WLH coals), coking coal (HZ coals), and long-flame coal (DL coals). The coal samples were collected from a freshly exposed mining face, sealed, and sent to the laboratory with minimal delay to prevent oxidation. The coal samples were crushed and screened to the appropriate quantity and sizes for each test. Prior to ScCO₂ treatment, all coal samples were dried at 80 °C for 48 h in a vacuum oven and divided into two even portions for comparative analysis: untreated and ScCO₂-treated coal.

Proximate analyses of moisture, ash, and volatile matter, measured using a 5E-MAG6600 proximate analyzer (Changsha Kaiyuan Instruments, China), were performed according to China National Standard GB/T 212-2008. The mean maximum reflectance of vitrinite ($R_{o,max}$ %) was determined using a Zeiss microscope-photometer (German) according to China National Standard GB/T 6948-2008. The basic properties of the coal samples are listed in Table 1.

Table 1. Basic Properties of the Coal Samples^a

sample	M_{ad} (%)	A_{ad} (%)	V_{ad} (%)	$R_{o,max}$ (%)
WLH	4.815	28.05	11.145	2.9246
HZ	0.665	16.115	21.725	1.5315
DL	6.565	18.43	42.215	0.6207

^a M_{ad} is the moisture content (air-dried basis), A_{ad} the ash content (air-dried basis), V_{ad} the volatile matter content (air-dried basis), and $R_{o,max}$ the maximum vitrinite reflectance.

2.2. High-Pressure Reaction Chamber for ScCO₂ Treatment.

To compare the measurements, ScCO₂ treatment of coal samples was conducted using a high-pressure reaction chamber. As shown in Figure 1, the apparatus consisted of a vacuum pump system, gas compression

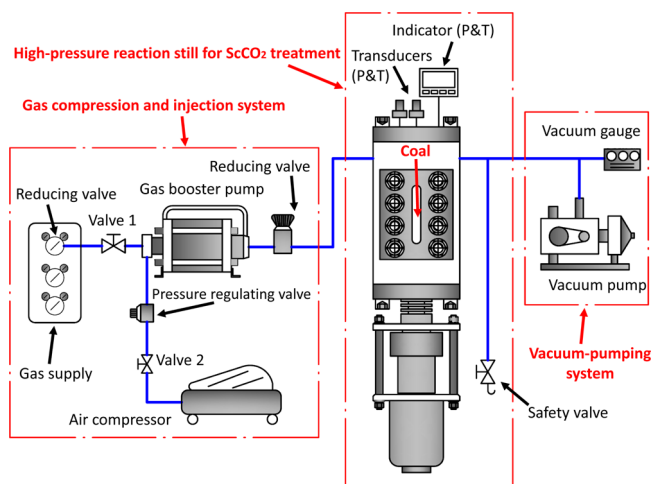


Figure 1. Schematic of the high-pressure reaction chamber used for ScCO₂ treatment.

and injection system, and high-pressure reaction chamber for ScCO₂ treatment. Prior to CO₂ injection, coal samples were degassed in the vacuum pump system (60 °C and 4 Pa for 24 h). When CO₂ is injected from the gas supply (from a steel cylinder), the air compressor began to work. After approximately 10 min, the gas booster pump was opened, and high-pressure CO₂ was transported to the high-pressure reaction chamber, with air compressor providing power, until the temperature and pressure indicators stabilized at 45 °C and 10 MPa, respectively. The experiment for ScCO₂ treatment was performed after equilibration for 240 h.

2.3. Experimental Methods. A PoreMaster 33 automated mercury intrusion porosimeter (Quantachrome Instruments, United States) was used to analyze the mesopore and macropore morphology of the coal samples. The MIP coal samples were sieved to a particle size range of 1–3 mm. MIP is the standard method to determine the PSD, pore volume, and surface area of coals, but it is more effective for macropores (>50 nm). Considering the potential destruction or compression effect on smaller pores (mesopores) caused by a higher mercury intruding pressure,³³ MIP with a relatively low mercury intruding pressure range (0.13–29.8 MPa) is considered more suitable for macropore measurements, corresponding to a pore diameter between 50 nm and 1.05×10^4 nm according to the Washburn equation.³⁴

The mesopore morphology was characterized by physisorption method (N₂ and CO₂ as probe molecules) using an automated Autosorb iQ2 gas sorption analyzer (Quantachrome Instruments, United States). The coal samples for N₂/CO₂ adsorption were ground to 0.2–0.25 mm. For N₂ adsorption at 77 K, the measurement of mesopores ranged from 2 to 50 nm, and good results were obtained from the N₂ adsorption isotherms at the relative pressures (P/P_0) ranging from 0.001 to 0.995. For micropore morphology analysis, CO₂ adsorption at 273 K may overcome the disadvantages of N₂

adsorption,¹⁵ where it is difficult to measure micropores of <2 nm. Because of the smaller molecular kinetic diameter and shorter adsorption equilibrium time, it is more accurate to obtain small pore diameters, especially in the range of 0.35–1.5 nm, within the micropore region. However, the micropore region between 1.5 and 2 nm is not easily analyzed using CO₂ adsorption. Despite these, CO₂ adsorption can mostly elucidate the changes in micropores.

A gas desorption experimental setup, as shown in Figure 2, was adopted to analyze the differences between untreated and ScCO₂-

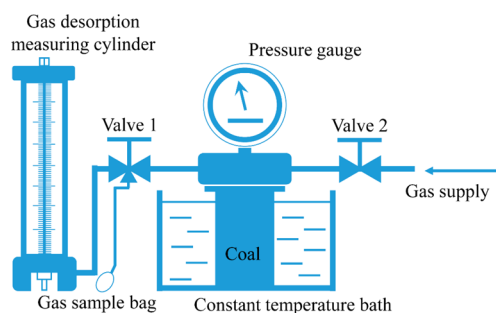


Figure 2. Gas desorption experimental setup.

treated coal samples, in compliance with China National Standards AQ/T 1065-2008 and GB 474-2008. The coal particles of the three coals ranging from 1 to 3 mm were placed in a container in a 60 °C water bath and connected to a vacuum pump in order to remove the pre-existing fluid from within the samples. After evacuation, methane (approximately 99.99% purity) was rapidly injected into the container in a 30 °C water bath for adsorption equilibrium. When the equilibrium reached a certain pressure, valve 1 was opened, and the gas was released to the atmosphere. Then, a gas volume measuring cylinder was connected to the container for the gas desorption experiment. The gas desorption volume and time data were recorded over 120 min to analyze the desorption properties.

3. RESULTS

3.1. Pore Volume and Surface Area. The most common method to determine mesopore specific surface area (SSA) and total pore volume (TPV) is N₂ adsorption using the Brunauer–Emmett–Teller (BET) and Barrett–Joyner–Halenda (BJH) models, respectively.^{35–37} The CO₂ adsorption data were interpreted using the Dubinin–Radushkevich (D–R) equation for micropore SSA and the Dubinin–Astakhov (D–A) equation for micropore TPV.^{38–40} These calculations can be performed automatically by the ASiQwin computer software from Quantachrome (United States). MIP-TPV and MIP-SSA were also calculated automatically by PoreMaster from Quantachrome, which is specialized for the analysis of macropores through MIP.

Table 2 summarizes the SSA, TPV, and porosity by CO₂ adsorption, N₂ adsorption, and MIP for untreated coals and coals after ScCO₂ treatment. In general, micropores and mesopores dominate in higher-ranked WLH coals, whereas lower-ranked DL coals are characterized by a greater number of macropores, but there is less development of macropores, mesopores, and micropores in intermediate-ranked HZ coals. After ScCO₂ treatment, the DA-TPV and DR-SSA values show an obvious decrease of 19.9% and 13.8% in higher-ranked WLH coals, as well as a slight decrease of 7.3% and 7.1% in intermediate-ranked HZ coals. The BJH-TPV and BET-SSA values of the mesopores determined by N₂ adsorption exhibit a similar trend with 30%, 11.9%, and 9.7% (precisely read) and 5.17% decreases in WLH and HZ coals, respectively. This result indicates that the accessibility of micropore and mesopore spaces in higher-ranked and intermediate-ranked coals decreased after ScCO₂ treatment. The decreased micropore accessibility caused by ScCO₂ may be associated with micropore and mesopore structure changes related to the change in the roughness degree of the coal surface on the pore morphology, which will be discussed later in this paper. For lower-ranked DL coals, however, micropores and mesopores show unique increases after ScCO₂ treatment, in contrast to WLH and HZ coals, with increases in DA-TPV and BJH-TPV of 12.5% and 33.3%, respectively. These differences may be related to the inherent nature of the highly volatile hydrocarbons in the lower-ranked coals. Previous studies^{31,41} proved that ScCO₂ may extract some organic compounds such as hydrocarbons, epoxy, aromatic hydrocarbon, etc. At this point, the extraction effect by ScCO₂ may be dominant in the DL coal compared with WLH and HZ coals. The MIP, MIP-TPV, and MIP-SSA of the macropores exhibit increasing trends for all three samples, as reflected by the porosity of 1.71%, 0.51%, and 1.06%, respectively. This indicates that ScCO₂ promoted the accessibility of macropores for all coals, which may also be influenced by mobilization of the removal of hydrocarbons.⁴² In addition, because of the majorities of micropores in high-rank coals and macropores in low-rank coals and the low porosity in middle-rank coals, the changes in TPV and SSA in WLH and DL coals are greater than those in HZ coals.

3.2. Pore Size Distribution. The TPV and SSA results are also reflected by the PSDs, including micropores (using DFT for CO₂ adsorption), mesopores (using DFT and BJH for N₂ adsorption), and macropores (using MIP), which were treated by ScCO₂. Generally, CO₂ adsorption using DFT (DFT-CO₂) represents the PSD of micropores (<2 nm) and submicropores (<0.8 nm). N₂ adsorption using DFT (DFT-N₂) primarily shows the lower pore size range of mesopores (<30 nm); N₂ adsorption using BJH (BJH-N₂) analyzes the PSD of

Table 2. Proximate and Petrographic Analyses of the Coal Samples^a

sample	measurement of micropores with CO ₂ adsorption		measurement of mesopores with N ₂ adsorption		measurement of macropores with MIP		
	DA-TPV (mL/g)	DR-SSA (m ² /g)	BJH-TPV (mL/g)	BET-SSA (m ² /g)	MIP-TPV (mL/g)	MIP-SSA (m ² /g)	porosity (%)
WLH-untreated	0.161	369.430	0.020	25.681	0.0032	0.149	4.47
WLH-SCCO ₂	0.129	318.497	0.014	22.634	0.0068	0.176	6.18
HZ-untreated	0.041	106.517	0.003	0.251	0.0032	0.2616	2.83
HZ-SCCO ₂	0.038	98.935	0.003	0.238	0.0045	0.2772	3.34
DL-untreated	0.072	202.759	0.006	3.853	0.0162	0.1805	7.21
DL-SCCO ₂	0.081	235.281	0.008	4.209	0.0182	0.2267	8.27

^aThe sample weight is on an air-dry base. SSA, specific surface area; TPV, total pore volume.

mesopores with a small range of macropores (<300 nm). Furthermore, there is a good representation of macropores (>50 nm). The ranges of the four PSD calculation methods are shown in Figure 3.

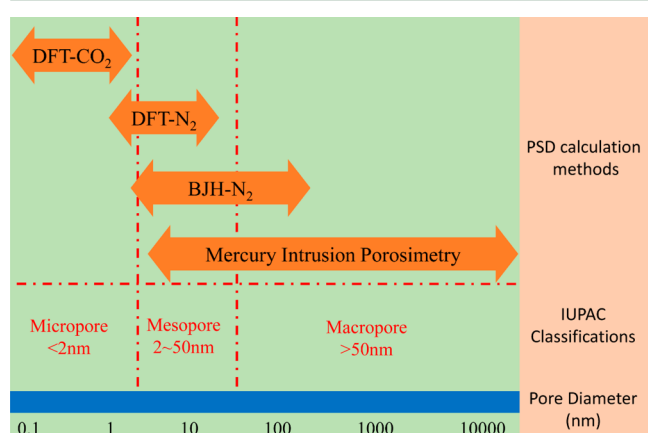


Figure 3. Methods for the measurement of porosity and pore size distribution (nm).

Figure 4 depicts the PSDs of untreated and ScCO₂-treated coal. It is obvious that the PSDs of the micropores and mesopores of WLH and HZ coals after ScCO₂ treatment are lower than those of the untreated coal according to the DFT-CO₂, DFT-N₂, and BJH-N₂ results, but the opposite trend is observed for DL coal. Meanwhile, the PSD of MIP after ScCO₂ treatment shows more macropores than untreated coal, which is consistent with the TPV and SSA results. Furthermore, the overall trends show that the PSD of HZ coals after ScCO₂ treatment exhibits less significant changes than those of the WLH and HZ coals. Additionally, it can be seen clearly in Figures 4 and 5 that BJH-N₂ and MIP are multimodal with respect to PSD, which means that within the coal samples there exists a discontinuous pore structure. For untreated coals, the blue circles in Figure 4 highlight a number of peaks. Table 3 summarizes and clarifies the positions and the changes in peak heights following ScCO₂-treatment. For untreated WLH, HZ, and DL coals, there were 3, 3, and 5 peaks on the DFT-CO₂ graph and 3, 5, and 2 peaks on the DFT-N₂ graph, respectively. After ScCO₂ treatment, some peaks were obviously changed and some were slightly changed. Moreover, the DFT-N₂ peak of HZ coal located at 3.44–4.25 nm vanished after ScCO₂ treatment, suggesting that ScCO₂ may alter the inherent structure of micropores and mesopores, making it possible to reduce or increase the TPV of coals. The decrease in micropores in WLH and HZ coals caused by ScCO₂ probably was well-explained by Yang et al.,⁴³ who reported that adsorption-induced deformation in pores may play an important role in the expansion of micropores with increasing CO₂ pressure. Eventually, small pores (such as micropores or smaller mesopores) may be transformed into larger pores (such as larger mesopores or macropores),^{12,44} resulting in increasing macropores, as shown in Figure 5.

Figure 5 shows the PSDs of the macropores for all coals determined by MIP before and after ScCO₂ treatment. WLH and HZ coals showed higher prominent peaks at 6.5 nm than that of DL coal, accompanied by a higher prominent peak at 2048 nm, which indicated that micropores and mesopores dominate in WLH coal, whereas DL coal contains more

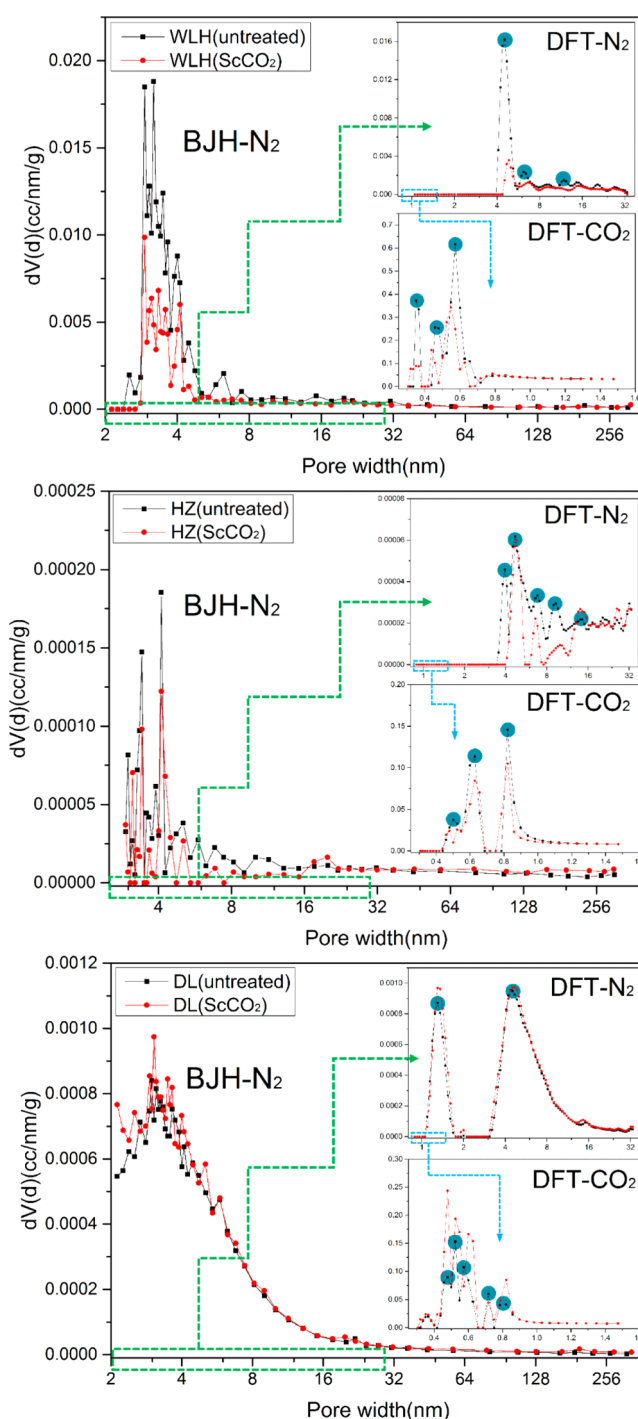


Figure 4. Pore size distribution of the untreated and ScCO₂-treated coal samples from the DFT and BJH analyses of N₂ and CO₂ adsorption.

macropores. With ScCO₂ treatment, the PSD of the macropores of HZ coal barely changed compared to those of the other two coals. These findings were in good agreement with the trend in the results in Table 2.

3.3. Fractal Dimension. It is generally accepted that fractal dimension provides useful information about the roughness of the coal surface. Fractal analysis can be performed using gas adsorption data and MIP.

For gas adsorption, the Neimark model⁴⁵ can accurately predict smaller pores (micropores) of fractal dimension on the

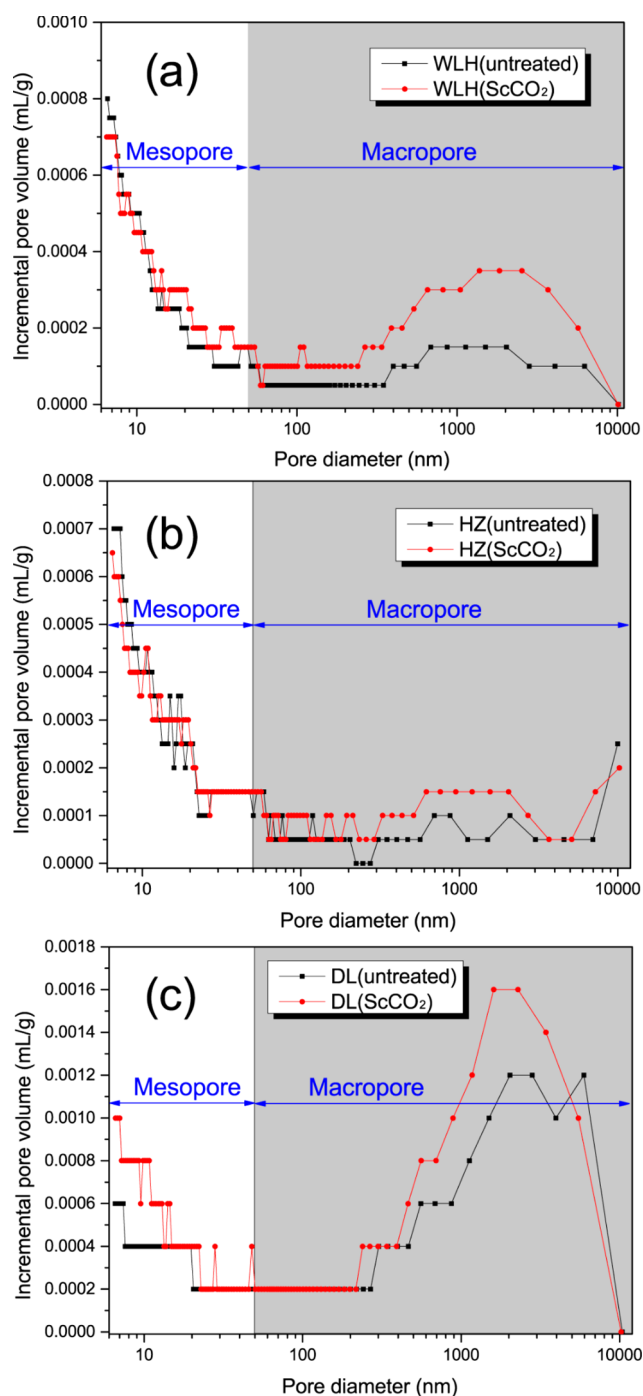


Figure 5. Pore size distribution of the untreated and ScCO_2 -treated coal samples from the MIP method: (a) WLH coal samples, (b) HZ coal samples, and (c) DL coal samples.

coal surface compared with the Avnir equation and FHH model, as demonstrated by Yao et al.⁴⁶ As shown in eq 1, the fractal dimension can be obtained via the Neimark model by

$$(D - 2)\log[r_c(P/P_0)] = C - \log[S(P/P_0)] \quad (1)$$

where D is the fractal dimension and C is a constant; $r_c(P/P_0)$ and $S(P/P_0)$ are the mean curvature radius and the area of the condensed liquid–gas interface at a given P/P_0 , respectively.

In this paper, N_2 adsorption data from P/P_0 intervals of 0–0.5 were adopted to calculate D , $r_c(P/P_0)$, and $S(P/P_0)$ using the Kiselev and Kelvin equations:

$$r_c(P/P_0) = 2\sigma\nu_m/RT\ln(P_0/P) \quad (2)$$

$$S(P/P_0) = (RT/\sigma) \int_{N(P/P_0)}^{N_{\max}} \ln(P_0/P) dN \quad (3)$$

where σ is the surface tension of the liquid adsorbate; ν_m is the molar volume of the liquid adsorbate; R is the universal gas constant; T is the temperature; $N(P/P_0)$ is a function of the equilibrium relative pressure at P/P_0 ; and N_{\max} is available as P approaches P_0 , representing the lower and upper limit of the integral. For MIP, the fractal dimension, at the scale of seepage pores (macropores), is calculated on the basis of Washburn equation, as reported by Friesen and Mikula.⁴⁷ Considering the compressibility effect on the deformation of the coal structure, the experimental data below 8 MPa were ignored, with pore radius ranging from 100 nm–40 000 nm.⁴⁸ Thus, the D values derived from the data where a straight line shows better fitting for all coals are reasonable in this range. The D value can be obtained from the slope of eq 4:

$$\log(dV/dP) = \log(k) + (D - 4)\log(P) \quad (4)$$

where V is the cumulative injection volume at a given pressure P and k is a proportional constant.

The results of the fractal dimension and correlation coefficients (R^2) obtained by gas adsorption and MIP are illustrated in Table 4. Overall, the D values of the two methods showed minima for intermediate-ranked HZ coals compared to higher-ranked WLH coals and lower-ranked DL coals. It has been demonstrated by Yao et al.⁴⁸ who reported that the fractal dimension decreased with increasing metamorphic grade of coal and then increased with coal rank.

Generally, the larger the fractal dimension, the rougher and more complex the pore surface and structure. For the Neimark model, the D values of WLH and HZ coals decreased after ScCO_2 treatment, which indicates that the pore surface became smoother. It has been proved that ScCO_2 makes the surface smoother through scanning electron microscopy (SEM).⁴⁹ The reason for the lower roughness may result from the changes in pore morphology, i.e., the transformation from smaller pores (micropores or mesopores) to larger pores (macropores). As previously shown in Figures 3–5 and Tables 2–4, the lower surface area and fewer micropores and mesopores of the WLH and HZ coals facilitate the development of macropores after ScCO_2 treatment, leading to the transformation. Additionally, the decrease in micropores makes the pore surface flatter and more regular,⁴⁸ which causes the decrease of the D value. However, the D value of DL coals increased slightly from 2.849 to 2.867, corresponding to the increase in the micropore surface due to the change in the micropore structure. For the D value calculated using MIP, the D values of all coals increased slightly (almost no change) and showed the same trend with coal rank as the Neimark model. This result indicates that larger pores become more complex and irregular after ScCO_2 treatment.

3.4. Pore Shape and Connectivity. Figure 6 shows the N_2 adsorption curves of WLH, HZ, and DL coals before and after ScCO_2 treatment. According to the classification of N_2 adsorption isotherms published by the IUPAC technical report,⁴⁷ all curves are identified as type II and IV(a), with a near-horizontal increase as the relative pressure approaches saturated vapor pressure ($P/P_0 = 1$). Although it is difficult to determine the pore shape of the samples because of the complexity of the coal structure, the hysteresis loop provides an

Table 3. Summary of the Position and Changes of Peaks after ScCO₂ Treatment Based on the PSDs in Figure 4^a

sample	peak number		position			
	DFT-CO ₂	DFT-N ₂	DFT-CO ₂	change	DFT-N ₂	change
WLH	3	3	0.31–0.38	↓↓↓	3.89–5.31	↓↓↓
			0.41–0.51	↓↓	5.77–6.82	↓
			0.52–0.60	↓↓	11.02–14.01	↓
HZ	3	5	0.43–0.54	↓	3.44–4.25	×
			0.54–0.68	↓↓	4.25–6.01	↓
			0.69–0.75	↓↓	6.13–7.89	↓↓
			0.74–0.90	↓↓	8.15–11.53	↓↓
					12.7–15.6	↑
DL	5	2	0.43–0.50	↑↑↑		
			0.50–0.55	↑↑		
			0.57–0.65	↑↑	1.05–1.76	↑
			0.69–0.75	↑	3.02–13.04	↑
			0.75–0.86	↑↑		

^aThe increase, decrease, and disappearance of peaks after ScCO₂ treatment are represented by the symbols “↑”, “↓”, and “×”, respectively. The number of symbols reflects the degree of the change.

Table 4. Fractal Dimension and Correlation Coefficients (R²) by Gas Adsorption and MIP Method

sample	NK model with gas adsorption method		calculation method based on Washburn equation with MIP	
	D	R ²	D	R ²
WLH-untreated	2.838	0.9945	2.953	0.9869
WLH-ScCO ₂	2.741	0.9916	2.954	0.9711
HZ-untreated	2.695	0.9963	2.749	0.9901
HZ-ScCO ₂	2.612	0.9972	2.751	0.9864
DL-untreated	2.849	0.9924	2.867	0.9912
DL-ScCO ₂	2.867	0.9960	2.868	0.9936

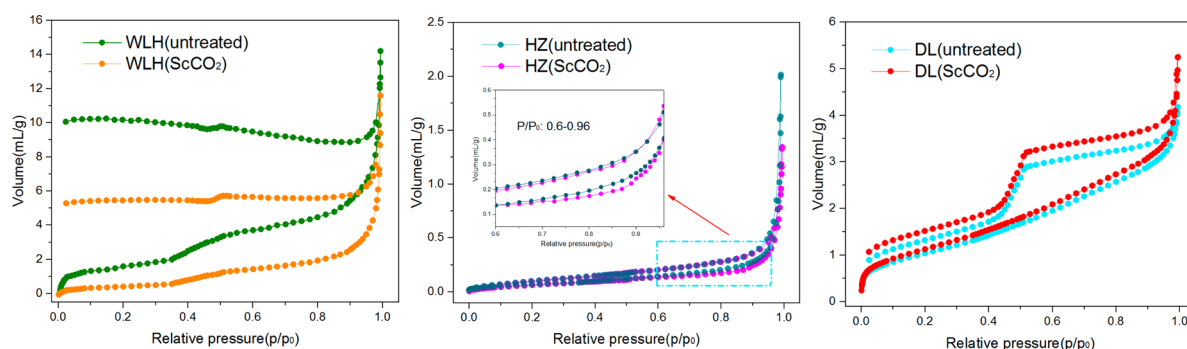
approximate assessment of the pore shape. On the basis of pore shape in coal, the types of pores can be classified as cylindrical, conical, slits, bottleneck, and interstices.⁵⁰ The hysteresis loop of DL coals at relative pressure between 0.43 and 0.997 is type H4, existing narrow slitlike pores. The low-pressure hysteresis of DL coals at relative pressure <0.43 may be related to the swelling of the nonrigid structure during gas adsorption. From an overall perspective of the hysteresis, there are a large number of conical pores in DL coals. In addition, there is an abrupt point in the desorption branch at relative pressure 0.5, which represents the minimum value of open pores. For HZ coals, discrepancies in the adsorption–desorption branches emerge at relative pressure greater than 0.5, indicating the presence of numerous cylindrical pores. There is also an inconspicuous

hysteresis loop, indicating the predominance of half-open or dead-end pores in the pore system. For WLH coals, there is a rapid growth in the adsorption branch with an apparent hysteresis loop in the adsorption–desorption isotherms. The pore system of WLH coals contains different levels of pore structure and size, which makes it complicated to classify the pore shape.

No obvious changes were observed in the pore shape for all coals with ScCO₂ treatment. However, the N₂ adsorption volume increased significantly for higher-ranked WLH coals and lower-ranked DL coals, accompanied by a slight change in intermediate-ranked HZ coals. These results were similar to the results mentioned above.

The changes in the CO₂ adsorption curves at 273 K on WLH, HZ, and DL coals before and after ScCO₂ treatment are shown in Figure 7. Overall, the curves for WLH and HZ coals exhibit convex surfaces, whereas the curve for DL coal is nearly a straight line. Then, higher-ranked WLH coals show the best gas adsorption capacity, followed by lower-ranked DL and intermediate-ranked HZ coals, and the changes in the adsorption volume after ScCO₂ treatment show the same trend as well. The decrease in the CO₂ adsorption of WLH and HZ coals represents a decrease in the accessibility of the micropores; however, the CO₂ adsorption increases noticeably for DL coals.

The cumulative pore volumes of the untreated and ScCO₂-treated coals analyzed by MIP demonstrate the injection and ejection processes in Figure 8. The connectivity of pores in coal

Figure 6. N₂ adsorption–desorption isotherms of the coal samples at 77 K before and after ScCO₂ treatment.

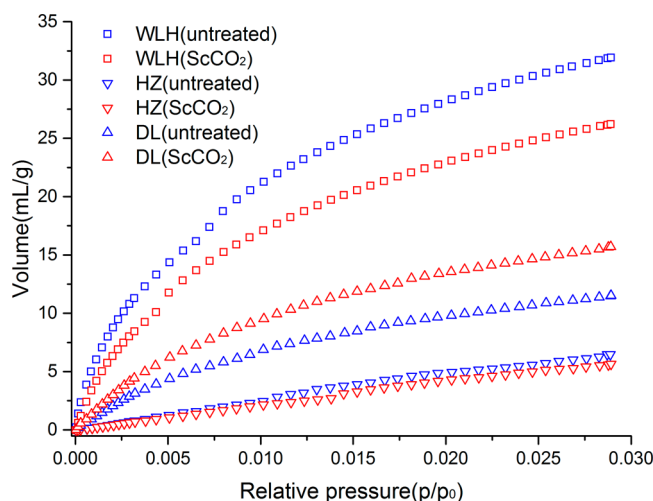


Figure 7. CO₂ adsorption isotherms of the coal samples at 273 K before and after ScCO₂ treatment.

can be classified as cross-linked, passing, or dead-end. Overall, the shape of all the ejection curves exhibit concave surfaces due to the numerous open and half-opened pores, which may impact the connectivity of pores. After ScCO₂ treatment, the injection volume of WLH coals increases by 21.4% (from 0.0234 to 0.0284 mL/g), while the injection volumes of HZ coals and DL coals increase by 16.7% (from 0.0198 to 0.0231 mL/g) and 27.2% (from 0.0378 to 0.0481 mL/g), respectively. Also, the changes in the ejection volume for WLH, HZ, and DL coals show similar trends, with an increase of 12.3% (from 0.0203 to 0.0228 mL/g), 6.3% (from 0.0221 to 0.0235 mL/g), and 23.6% (from 0.0296 to 0.0366 mL/g), suggesting an increase in the open pore volume after ScCO₂ treatment.⁵¹ Moreover, the hysteresis of all coals increased after ScCO₂ treatment, which prevented mercury from extruding out of pores, indicating that the pore system had become more complex with more bottleneck pores (one example is the ink-bottle pore). In short, ScCO₂ treatment causes an increase in the number of open pores and half-opened pores, contributing to the development of effective pores to some extent. Taken in conjunction with the increase in macropores and the decrease in mesopores and micropores in pore structure as mentioned above, this result may contribute to the characteristics and connectivity of the pore structure related to desorption, diffusion, and seepage.^{52,53}

4. DISCUSSION OF THE MECHANISM OF DESORPTION PROCESS AND ITS EFFECTS ON LONG-TERM STORAGE

Coal is an important reservoir for long-term CO₂ storage because the types of pores play a meaningful role in gas adsorption, desorption, diffusion, and seepage in coal seams. The results of the changes in pore morphology have shown that ScCO₂ treatment decreases the number of micropores and promotes the accessibility of macropores, which makes a transformation to larger pores. The effect of extraction by ScCO₂ facilitates the production of effective pores and the connectivity of the pore structure in coal. It has been proven that the adsorption process is the dominant form of gas storage in coal, but investigations of the gas desorption mechanism during CO₂ sequestration are still limited. Further emphasis should be placed on the mechanism of desorption process after

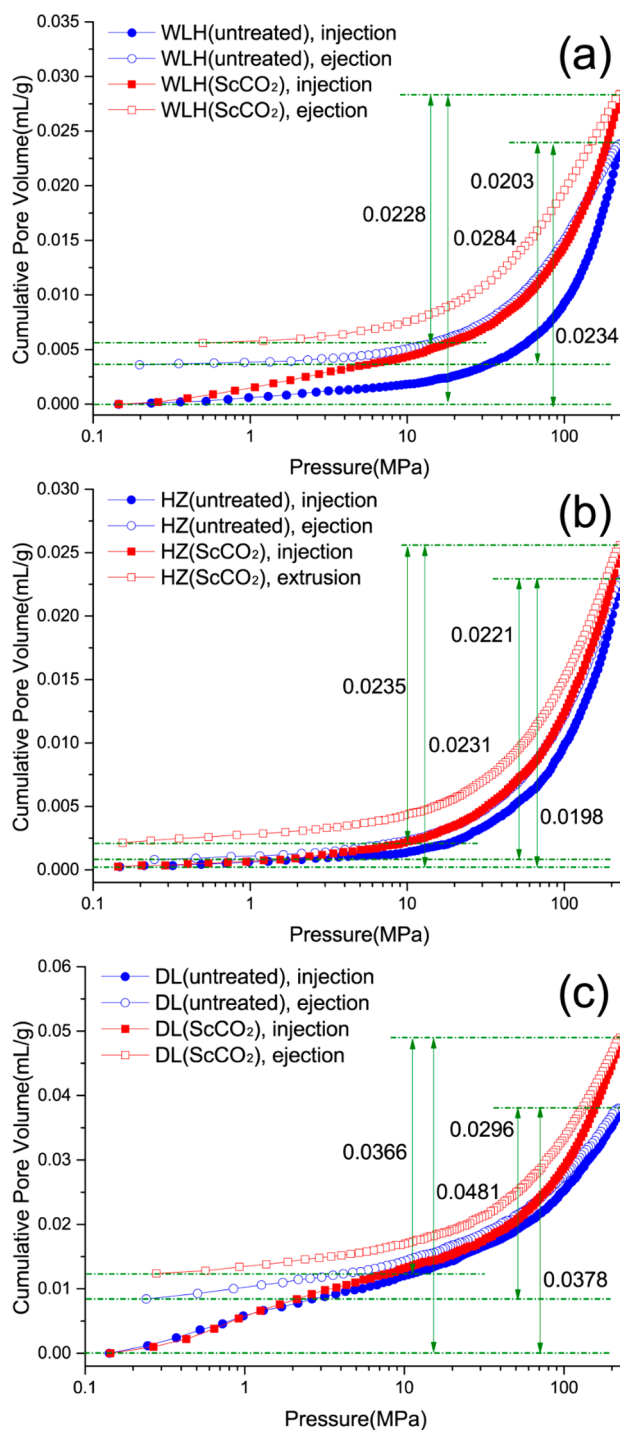


Figure 8. MIP curves of the coal samples before and after ScCO₂ treatment: (a) WLH coal samples, (b) HZ coal samples, and (c) DL coal samples.

ScCO₂ treatment to explore the influence on long-term CO₂ storage. Hence, the desorption properties of gas desorption curves were performed and analyzed.

4.1. Mechanism of Desorption Process. The gas desorption curves of WLH, HZ, and DL coals for 120 min are displayed in Figure 9. The gas pressure in the pores suddenly returns to atmospheric pressure via desorption, which initially occurs in larger pores (macropores).⁵⁴ The gas desorption rate in the first 10 min is relatively higher, with the desorption volume accounting for nearly 50% of the total. It

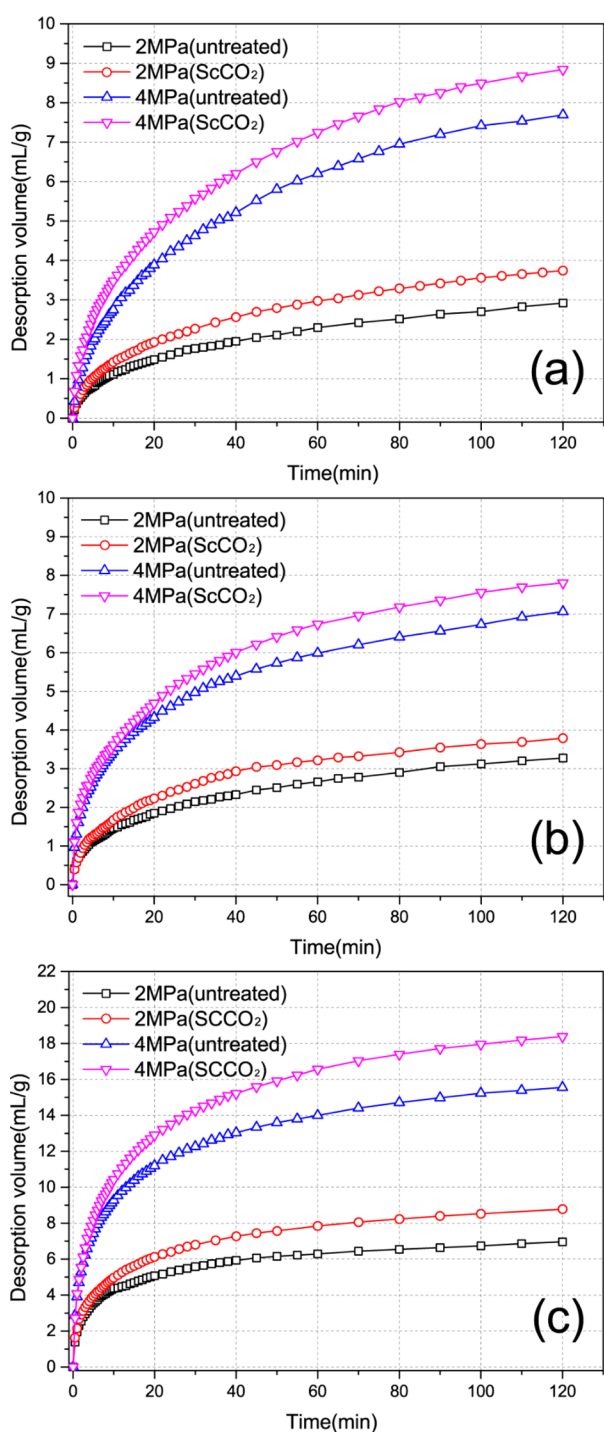


Figure 9. Methane desorption curves of untreated and ScCO₂-treated coal samples under different equilibrium pressures: (a) WLH coal samples, (b) HZ coal samples, and (c) DL coal samples.

then gradually decreases with time. Also, it can be seen that lower-ranked DL coals have a higher desorption rate, followed by intermediate-ranked HZ coals and higher-ranked WLH coals, indicating a relationship between the coal structure evolution and the degree of metamorphism.⁵⁵ At the equilibrium pressure of 4 MPa, the curves for all coals exhibit total desorption volumes higher than those at 2 MPa. This is because the initial gas concentration increases with more adsorption amount at higher equilibrium pressure before the

desorption process, and a higher gas concentration gradient accelerates the faster gas diffusion speeds.⁵⁶

After ScCO₂ treatment, the total desorption volume of all coals increased compared to untreated coals, which may be attributed to the increase in macropores and connectivity in the pore network, as mentioned earlier. It is worth mentioning that the difference in the total desorption volume between untreated and ScCO₂-treated curves at the equilibrium pressure of 4 MPa is greater than that at the equilibrium pressure of 2 MPa, which can be explained as follows.

Before desorption, the adsorption equilibrium process was performed necessarily over a long period of time (2–3 days). During this period, adsorption behavior does not occur unless gas molecules have sufficient energy to enter the pore network. Physically constricted pore spaces, which may generate energy barrier on molecules, exist in the mouths or necks of pores (commonly in micropores, mesopores, and macropores).^{22,57} In this case, higher pressure, sufficient equilibrium time, and higher temperature are conventional ways to overcome the barrier, with the purpose of adsorption equilibrium.⁵⁸

It has been previously proven that volatile constituents, existing in the pore mouths or necks, are the main contributors to the energy barrier and physical constriction.⁵⁹ The major components include polyaromatic, aliphatic, and aromatic hydrocarbons, which impact the connectivity of the pore structure. It can be also found that ScCO₂ may change the coal structure by dissolving and mobilizing hydrocarbons in the coal matrix, resulting in decreased volatile constituents in the constricted pores.⁴¹ Consequently, the physically constricted pore spaces are opened completely with the improvement in pore connectivity, which has been demonstrated by the experimental results (section 3) presented in this paper.

Figure 10 illustrates the mechanism of the desorption process in the constricted pores of the coal matrix for the untreated,

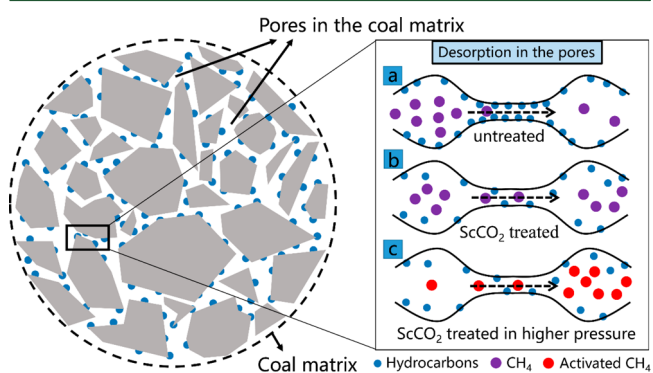


Figure 10. A conceptual model of the desorption process mechanism on constricted pores in the coal matrix under the conditions of ScCO₂ and high pressure.

ScCO₂-treated, and ScCO₂-treated at higher pressure conditions. Blue circles represent hydrocarbon molecules in the coal matrix, purple circles methane molecules, and red circles activated methane molecules with sufficient energy at higher pressure. In the adsorption equilibrium process before adsorption, without ScCO₂ treatment, more hydrocarbons may be present in the pore mouths or necks, leading to the increase in energy barrier on molecules. Afterward when gas desorption occurs over a period of 120 min, the constricted pores were made inaccessible to methane molecules to move across during desorption process, as shown on Figure 10a.

However, ScCO₂ treatment reduces the energy barrier by extracting and mobilizing hydrocarbons, which facilitates the movement of methane molecules, as shown in Figure 10b. This can explain why the total desorption volumes of the ScCO₂-treated curves are greater than those of the untreated curves in Figure 9. Moreover, at higher equilibrium pressure (4 MPa), more gas molecules are possibly activated at the dual condition of ScCO₂ treatment and higher pressure; thus, enough molecules participate in the desorption process via the pores that were newly opened (Figure 10c) with the effect of extraction. This explanation may confirm the results that the difference in total desorption volume between untreated and ScCO₂ curves at 4 MPa is greater than that at 2 MPa, as shown in Figure 9. In addition, there is a negative relationship between volatile matter and the metamorphic grade of coals, that is, lower-ranked coals have higher volatile contents than higher-ranked coals. For DL coals, ScCO₂ extracted and mobilized more volatile hydrocarbons than in WLH and HZ coals, so the increase in total desorption volume of DL coals between untreated and ScCO₂-treated curves is greater than that of WLH and HZ coals.

4.2. Influence of ScCO₂ on Long-Term Sequestration.

In this study, the influence of ScCO₂ on long-term sequestration is reflected by two characteristics: pore morphology and desorption properties. The former are mainly related to the promotion of the seepage pore (macropore) development, making it more accessible on the scale of coal seams. Also, it may enhance the connectivity of the pore structure, leading to a direct impact on the latter, i.e., types of pores, including constricted pores. Thus, in coal reservoirs, more constricted pores become more accessible after ScCO₂ extraction. In this scenario, CH₄ molecules are more inclined to move from the coal matrix via desorption and diffusion and be transported in the fracture via seepage. These two aspects after ScCO₂ treatment could have positive effects on the permeability of the target coal seams and practical ECBM projects during long-term storage.

5. CONCLUSIONS

In this paper, high-, middle- and low-rank coals were investigated to determine the influences of ScCO₂ on the pore morphology. A high-pressure reaction chamber was adopted for the preparation of ScCO₂-treated coal. The morphology of the micropores, mesopores, and macropores in the samples were analyzed using CO₂ adsorption, N₂ adsorption, and MIP, respectively. The gas desorption properties of untreated and ScCO₂-treated coals were evaluated to verify the influence of ScCO₂ on the pore morphology. Finally, the implications of these results for CO₂ geological sequestration were discussed. Major findings are summarized as follows:

(1) With ScCO₂ treatment, for high- and middle-rank coals, micropores (DA-TPV and DR-SSA), as analyzed by CO₂ adsorption, and mesopores (BJH-TPV and BET-SSA), as analyzed by N₂ adsorption, decreased, whereas they increased for low-rank coals. The development of macropores (MIP-TPV and MIP-SSA) for all coals was promoted by ScCO₂. The PSD results revealed the same trends. There were significant changes in high-rank coals, smaller changes in middle-rank coals, and only slight changes in low-rank coals.

(2) For high- and middle-rank coals, the decrease in the *D* values after ScCO₂ treatment demonstrated that the surfaces of the smaller pores (micropores or mesopores) became smoother

and transformed into larger pores (macropores). For high-rank coals, the larger pores became more complex and irregular after ScCO₂ treatment. ScCO₂ caused slight changes in the pore shape for all coals. However, the effect of organic liquid extraction by ScCO₂ facilitated the development of more effective pores and greater connectivity of the pore structure in the coal.

(3) The desorption properties for all coals were improved by ScCO₂ treatment, and the difference in the total desorption volume between untreated and ScCO₂-treated curves at the equilibrium pressure of 4 MPa was greater than that at the equilibrium pressure of 2 MPa. This can be explained by a conceptual model associated with the migration mechanism of CO₂ molecules in the constricted pore spaces of the coal matrix at higher pressure and with ScCO₂ treatment. The results have implications for CO₂ geological sequestration and CO₂-ECBM.

AUTHOR INFORMATION

Corresponding Author

*E-mail: cyp620924@hotmail.com. Tel: +86-516-83885948. Fax: +86-516-83995097.

ORCID

Yuanping Cheng: [0000-0001-8208-193X](https://orcid.org/0000-0001-8208-193X)

Notes

The authors declare no competing financial interest.

ACKNOWLEDGMENTS

The authors are grateful to the Fundamental Research Funds for the Central Universities (2017XKZD01) and the Priority Academic Program Development of Jiangsu Higher Education Institutions (PAPD).

REFERENCES

- (1) *BP Statistical Review of World Energy*; British Petroleum: London, 2012.
- (2) Barker, R.; Hua, Y.; Neville, A. Internal corrosion of carbon steel pipelines for dense-phase CO₂ transport in carbon capture and storage (CCS)—a review. *Int. Mater. Rev.* **2017**, *62*, 1–31.
- (3) Goodman, A.; Campus, L.; Schroeder, K. Direct evidence of carbon dioxide sorption on Argonne premium coals using attenuated total reflectance-Fourier transform infrared spectroscopy. *Energy Fuels* **2005**, *19* (2), 471–476.
- (4) Perera, M.; Ranjith, P.; Choi, S.-K.; Bouazza, A.; Kodikara, J.; Airey, D. A review of coal properties pertinent to carbon dioxide sequestration in coal seams: with special reference to Victorian brown coals. *Environ. Earth Sci.* **2011**, *64* (1), 223–235.
- (5) White, C. M.; Smith, D. H.; Jones, K. L.; Goodman, A. L.; Jikich, S. A.; LaCount, R. B.; DuBose, S. B.; Ozdemir, E.; Morsi, B. I.; Schroeder, K. T. Sequestration of carbon dioxide in coal with enhanced coalbed methane recovery a review. *Energy Fuels* **2005**, *19* (3), 659–724.
- (6) Karacan, C. Ö.; Mitchell, G. D. Behavior and effect of different coal microlithotypes during gas transport for carbon dioxide sequestration into coal seams. *Int. J. Coal Geol.* **2003**, *53* (4), 201–217.
- (7) Ozdemir, E. Modeling of coal bed methane (CBM) production and CO₂ sequestration in coal seams. *Int. J. Coal Geol.* **2009**, *77* (1), 145–152.
- (8) Perera, M.; Ranjith, P.; Choi, S.; Airey, D.; Weniger, P. Estimation of gas adsorption capacity in coal: a review and an analytical study. *Int. J. Coal Prep. Util.* **2012**, *32* (1), 25–55.
- (9) Yong, Z.; Mata, V.; Rodrigues, A. r. E. Adsorption of carbon dioxide at high temperature—a review. *Sep. Purif. Technol.* **2002**, *26* (2), 195–205.
- (10) Clarkson, C.; Bustin, R. The effect of pore structure and gas pressure upon the transport properties of coal: a laboratory and

- modeling study. 2. Adsorption rate modeling. *Fuel* **1999**, *78* (11), 1345–1362.
- (11) Liu, Y.; Wilcox, J. Effects of surface heterogeneity on the adsorption of CO₂ in microporous carbons. *Environ. Sci. Technol.* **2012**, *46* (3), 1940–1947.
- (12) Zhang, D.; Gu, L.; Li, S.; Lian, P.; Tao, J. Interactions of supercritical CO₂ with coal. *Energy Fuels* **2013**, *27* (1), 387–393.
- (13) Rouquerol, J.; Avnir, D.; Fairbridge, C.; Everett, D.; Haynes, J.; Pernicone, N.; Ramsay, J.; Sing, K.; Unger, K. Recommendations for the characterization of porous solids (Technical Report). *Pure Appl. Chem.* **1994**, *66* (8), 1739–1758.
- (14) Thommes, M.; Kaneko, K.; Neimark, A. V.; Olivier, J. P.; Rodriguez-Reinoso, F.; Rouquerol, J.; Sing, K. S. Physisorption of gases, with special reference to the evaluation of surface area and pore size distribution (IUPAC Technical Report). *Pure Appl. Chem.* **2015**, *87* (9–10), 1051–1069.
- (15) Clarkson, C.; Bustin, R. The effect of pore structure and gas pressure upon the transport properties of coal: a laboratory and modeling study. 1. Isotherms and pore volume distributions. *Fuel* **1999**, *78* (11), 1333–1344.
- (16) Karacan, C.; Okandan, E. Adsorption and gas transport in coal microstructure: investigation and evaluation by quantitative X-ray CT imaging. *Fuel* **2001**, *80* (4), 509–520.
- (17) Liu, J.; Jiang, X.; Huang, X.; Wu, S. Morphological characterization of super fine pulverized coal particle. Part 4. Nitrogen adsorption and small angle X-ray scattering study. *Energy Fuels* **2010**, *24* (5), 3072–3085.
- (18) Zhai, C.; Qin, L.; Liu, S.; Xu, J.; Tang, Z.; Wu, S. Pore Structure in Coal: Pore Evolution after Cryogenic Freezing with Cyclic Liquid Nitrogen Injection and Its Implication on Coalbed Methane Extraction. *Energy Fuels* **2016**, *30* (7), 6009–6020.
- (19) Liu, S.-Q.; Sang, S.-X.; Liu, H.-H.; Zhu, Q.-P. Growth characteristics and genetic types of pores and fractures in a high-rank coal reservoir of the southern Qinshui basin. *Ore Geol. Rev.* **2015**, *64*, 140–151.
- (20) Marsh, H. Adsorption methods to study microporosity in coals and carbons—a critique. *Carbon* **1987**, *25* (1), 49–58.
- (21) Meyers, R. *Coal Structure*; Elsevier: Amsterdam, 2012.
- (22) Cui, X.; Bustin, R. M.; Dipple, G. Selective transport of CO₂, CH₄, and N₂ in coals: insights from modeling of experimental gas adsorption data. *Fuel* **2004**, *83* (3), 293–303.
- (23) Larsen, J. W. The effects of dissolved CO₂ on coal structure and properties. *Int. J. Coal Geol.* **2004**, *57* (1), 63–70.
- (24) Viète, D.; Ranjith, P. The effect of CO₂ on the geomechanical and permeability behaviour of brown coal: implications for coal seam CO₂ sequestration. *Int. J. Coal Geol.* **2006**, *66* (3), 204–216.
- (25) Span, R.; Wagner, W. A new equation of state for carbon dioxide covering the fluid region from the triple-point temperature to 1100 K at pressures up to 800 MPa. *J. Phys. Chem. Ref. Data* **1996**, *25* (6), 1509–1596.
- (26) Lucht, L. M.; Larson, J. M.; Peppas, N. A. Macromolecular structure of coals. 9. Molecular structure and glass transition temperature. *Energy Fuels* **1987**, *1* (1), 56–58.
- (27) Giri, C.; Sharma, D. Mass-transfer studies of solvent extraction of coals in N-methyl-2-pyrrolidone. *Fuel* **2000**, *79* (5), 577–585.
- (28) Painter, P.; Starsinic, M.; Coleman, M. Determination of functional groups in coal by Fourier transform interferometry. *Fourier Transform Infrared Spectroscopy* **1985**, *4*, 169–240.
- (29) Day, S.; Fry, R.; Sakurovs, R. Swelling of Australian coals in supercritical CO₂. *Int. J. Coal Geol.* **2008**, *74* (1), 41–52.
- (30) Sakanishi, K.; Watanabe, I.; Nonaka, T.; Kishino, M.; Mochida, I. Effects of organic acid pretreatment on the structure and pyrolysis reactivity of coals. *Fuel* **2001**, *80* (2), 273–281.
- (31) Kolak, J. J.; Burruss, R. C. Geochemical investigation of the potential for mobilizing non-methane hydrocarbons during carbon dioxide storage in deep coal beds. *Energy Fuels* **2006**, *20* (2), 566–574.
- (32) Kumar, M.; Shankar, R. H. Removal of ash from Indian Assam coking coal using sodium hydroxide and acid solutions. *Energy Sources* **2000**, *22* (2), 187–196.
- (33) Chen, Q.; Zhang, J.; Tang, X.; Li, W.; Li, Z. Relationship between pore type and pore size of marine shale: An example from the Sinian–Cambrian formation, upper Yangtze region, South China. *Int. J. Coal Geol.* **2016**, *158*, 13–28.
- (34) Washburn, E. W. The dynamics of capillary flow. *Phys. Rev.* **1921**, *17* (3), 273.
- (35) Barrett, E. P.; Joyner, L. G.; Halenda, P. P. The determination of pore volume and area distributions in porous substances. I. Computations from nitrogen isotherms. *J. Am. Chem. Soc.* **1951**, *73* (1), 373–380.
- (36) Brunauer, S.; Emmett, P.; Teller, E. Absorption of gases in multimolecular layers. *J. Am. Chem. Soc.* **1938**, *60*, 309–319.
- (37) Yao, Y.; Liu, D.; Tang, D.; Tang, S.; Che, Y.; Huang, W. Preliminary evaluation of the coalbed methane production potential and its geological controls in the Weibei Coalfield, Southeastern Ordos Basin, China. *Int. J. Coal Geol.* **2009**, *78* (1), 1–15.
- (38) Dubinin, M.; Astakhov, V. Description of adsorption equilibria of vapors on zeolites over wide ranges of temperature and pressure. In *Advances in Chemistry*; American Chemical Society: Washington, DC, 1971; pp 69–85.
- (39) Dubinin, M.; Radushkevich, L. Equation of the characteristic curve of activated charcoal. *Chem. Zentralbl.* **1947**, *1* (1), 875.
- (40) Gasparik, M.; Bertier, P.; Gensterblum, Y.; Ghanizadeh, A.; Krooss, B. M.; Littke, R. Geological controls on the methane storage capacity in organic-rich shales. *Int. J. Coal Geol.* **2014**, *123*, 34–51.
- (41) Kolak, J. J.; Hackley, P. C.; Ruppert, L. F.; Warwick, P. D.; Burruss, R. C. Using ground and intact coal samples to evaluate hydrocarbon fate during supercritical CO₂ injection into coal beds: Effects of particle size and coal moisture. *Energy Fuels* **2015**, *29* (8), 5187–5203.
- (42) Monin, J.; Barth, D.; Perrut, M.; Espitalie, M.; Durand, B. Extraction of hydrocarbons from sedimentary rocks by supercritical carbon dioxide. *Org. Geochem.* **1988**, *13* (4), 1079–1086.
- (43) Yang, K.; Lu, X.; Lin, Y.; Neimark, A. V., Effects of CO₂ adsorption on coal deformation during geological sequestration. *J. Geophys. Res.* **2011**, *116*, (B8). DOI: [10.1029/2010JB008002](https://doi.org/10.1029/2010JB008002).
- (44) Wang, Q.; Zhang, D.; Wang, H.; Jiang, W.; Wu, X.; Yang, J.; Huo, P. Influence of CO₂ Exposure on High-Pressure Methane and CO₂ Adsorption on Various Rank Coals: Implications for CO₂ Sequestration in Coal Seams. *Energy Fuels* **2015**, *29* (6), 3785–3795.
- (45) Neimark, A. V.; Unger, K. K. Method of discrimination of surface fractality. *J. Colloid Interface Sci.* **1993**, *158* (2), 412–419.
- (46) Yao, Y.; Liu, D.; Tang, D.; Tang, S.; Huang, W. Fractal characterization of adsorption-pores of coals from North China: an investigation on CH₄ adsorption capacity of coals. *Int. J. Coal Geol.* **2008**, *73* (1), 27–42.
- (47) Friesen, W.; Mikula, R. Fractal dimensions of coal particles. *J. Colloid Interface Sci.* **1987**, *120* (1), 263–271.
- (48) Yao, Y.; Liu, D.; Tang, D.; Tang, S.; Huang, W.; Liu, Z.; Che, Y. Fractal characterization of seepage-pores of coals from China: an investigation on permeability of coals. *Comput. Geosci.* **2009**, *35* (6), 1159–1166.
- (49) Gathitu, B. B.; Chen, W.-Y.; McClure, M. Effects of coal interaction with supercritical CO₂: physical structure. *Ind. Eng. Chem. Res.* **2009**, *48* (10), 5024–5034.
- (50) Guo, H.; Cheng, Y.; Yuan, L.; Wang, L.; Zhou, H. Unsteady-state diffusion of gas in coals and its relationship with coal pore structure. *Energy Fuels* **2016**, *30* (9), 7014–7024.
- (51) Wang, H.; Fu, X.; Jian, K.; Li, T.; Luo, P. Changes in coal pore structure and permeability during N₂ injection. *J. Nat. Gas Sci. Eng.* **2015**, *27*, 1234–1241.
- (52) Sang, S.; Xu, H.; Fang, L.; Li, G.; Huang, H. Stress relief coalbed methane drainage by surface vertical wells in China. *Int. J. Coal Geol.* **2010**, *82* (3), 196–203.
- (53) Zhang, S.; Tang, S.; Tang, D.; Pan, Z.; Yang, F. The characteristics of coal reservoir pores and coal facies in Liulin district, Hedong coal field of China. *Int. J. Coal Geol.* **2010**, *81* (2), 117–127.

(54) Zhao, W.; Cheng, Y.; Jiang, H.; Jin, K.; Wang, H.; Wang, L. Role of the rapid gas desorption of coal powders in the development stage of outbursts. *J. Nat. Gas Sci. Eng.* **2016**, *28*, 491–501.

(55) An, F.-h.; Cheng, Y.-p.; Wu, D.-m.; Li, W. Determination of Coal Gas Pressure Based on Characteristics of Gas Desorption [J]. *J. Min. Saf. Eng.* **2011**, *1*, 18.

(56) Jiang, H.; Cheng, Y.; Yuan, L. A Langmuir-like desorption model for reflecting the inhomogeneous pore structure of coal and its experimental verification. *RSC Adv.* **2015**, *5* (4), 2434.

(57) Koresh, J. E.; Kim, T.; Koros, W. Study of ultramicroporous carbons by high-pressure sorption. Part 1.—N₂, CO₂, O₂ and He isotherms. *J. Chem. Soc., Faraday Trans. 1* **1989**, *85* (7), 1537–1544.

(58) Nguyen, T. X.; Bhatia, S. K. Determination of pore accessibility in disordered nanoporous materials. *J. Phys. Chem. C* **2007**, *111* (5), 2212–2222.

(59) Bae, J.-S.; Bhatia, S. K.; Rudolph, V.; Massarotto, P. Pore accessibility of methane and carbon dioxide in coals. *Energy Fuels* **2009**, *23* (6), 3319–3327.